We are IntechOpen, the world's leading publisher of Open Access books Built by scientists, for scientists

4,800
Open access books available

122,000
International authors and editors

135M
Downloads

Our authors are among the

154
Countries delivered to

TOP 1%
most cited scientists

12.2%
Contributors from top 500 universities

CLARIVATE ANALYTICS BOOK CITATION INDEX INDEXED

WEB OF SCIENCE™

Selection of our books indexed in the Book Citation Index in Web of Science™ Core Collection (BKCI)

Interested in publishing with us?
Contact book.department@intechopen.com

Numbers displayed above are based on latest data collected.
For more information visit www.intechopen.com

24

Strain variations on rolling condition in accumulative roll-bonding by finite element analysis

Tadanobu INOUE
National Institute for Materials Science, Japan

1. Introduction

Bulk ultrafine-grained (UFG) materials with grain sizes of tens to hundreds of nanometers showing improved mechanical properties without the addition of alloying elements have attracted the attention of researchers in materials science (Inoue et al., 2010a; Kimura et al., 2008), and microstructural evolution and hardness variation in the UFG materials fabricated by a plastic deformation process such as equal-channel angular pressing (ECAP) (Horita et al., 2000; Segal, 1995), accumulative roll bonding (ARB) (Saito et al., 1998), caliber rolling (Inoue et al., 2007b; 2009c; Mukai et al., 2010), and high-pressure torsion (HPT) shown in Fig. 1, have been studied in detail (Inoue et al., 2009a; 2010b; Todaka et al., 2008). Since the microstructural evolution of plastically deformed materials is directly related to the magnitude of plastic deformation, the understanding of the phenomenon associated with the strain development is very important (Inoue et al., 2001; 2007a; 2008). For example, in ARB which is a severe plastic deformation process for realizing UFG microstructures in metals and alloys, the microstructure and texture in a sheet processed by one ARB cycle without lubricant dramatically change depending on the thickness location of the sheet (Kamikawa et al., 2007). In a rolling process, including ARB, it is reported that these changes are caused by the redundant shear strain imposed by large friction between rolls and sheet.

Rolling is an excellent plastic deformation process in the mass production of a metallic sheet, and many reports have been published regarding the rolling characteristics, shape control, and microstructure control through theory, numerical simulations, and many experiments. Figure 2 shows a typical illustration of a rolling process. The classical rolling theory (Underwood, 1952) has been used as a method to qualitatively understand variations of the rolling characteristics of a rolling force and torque against the processing parameters such as the roll diameter, reduction, rolling speed, and friction condition. On the other hand, deformation in sheet metals by rolling has been studied in detail through many experiments and finite element simulations. Flow of metals in rolling experiments makes the presence of the shear deformation clear and qualitative relation between equivalent strain including shear deformation and microstructure through sheet thickness has been reported in the literature (Lee et al., 2002; Sakai et al., 1988; Matsuoka et al., 1997). However, only a few

studies have been carried out on quantitative correlation between microstructure and strain through a combination of experiments and finite element simulations (Um et al., 2000; Mukhopadhyay et al., 2007). The embedded-pin method (see Fig. 3) is often employed to measure the shear strain through thickness experimentally (Cui & Ohori, 2000; Hashimoto et al., 1998), but magnitude of shear strain and equivalent strain obtained by this method do not exhibit the exact value (Inoue & Tsuji, 2009b). Therefore, for controlling the microstructures, it is essential to understand the deformation behavior in the sheet accurately and quantitatively through a combination of rolling experiments and finite element simulations.

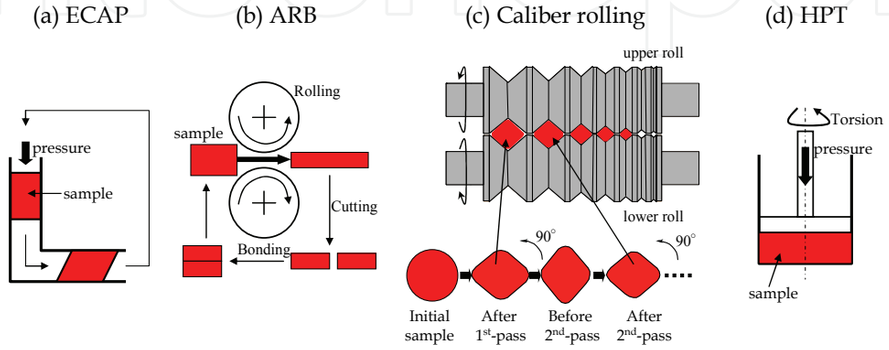

Fig. 1. Major severe plastic deformation processes.

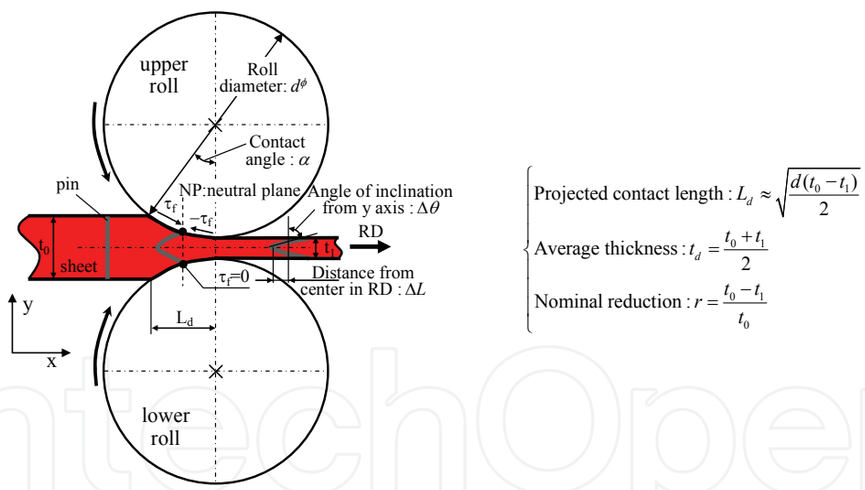

Fig. 2. Schematic illustration showing the geometry of the rolling process.

The shear strain is caused by not only the friction between the rolls and the material surface but also the roll bite geometry, L_d/t_d (Backofen, 1972; Dieter, 1988). Here, L_d denotes the projected length of the contact arc to the horizontal plane, and t_d is the average sheet thickness shown in Fig. 2. In interstitial free (IF) steel sheets rolled by 50% with and without lubrication, Um et al., 2000 investigated the variations of the strain distribution and the flection of an embedded pin against the roll bite geometry by changing the initial sheet thickness and roll diameter. However, the distribution of the shear strain is not shown and

the effect of the roll bite geometry on strain distribution in sheet rolling is not systematically studied. Furthermore, it is not verified that the roll bite geometry is a universal parameter on the strain distribution under unlubricated condition. Hence, it is important to systematically explore the effect of the L_d/t_d ratio on the magnitude and distribution of strains under various friction conditions using numerical simulations. Moreover, if the magnitude and distribution of strains through the thickness in a rolled sheet can be quantitatively estimated by using experimental data (Kamikawa et al., 2007; Sakai et al., 1988), ΔL and $\Delta\theta$, measured from the embedded-pin method, as shown in Fig. 3, a simulation result would provide useful guidelines for analyzing the evolution of microstructures in the ARB process as well as designing the microstructure of the sheet metal by conventional rolling.

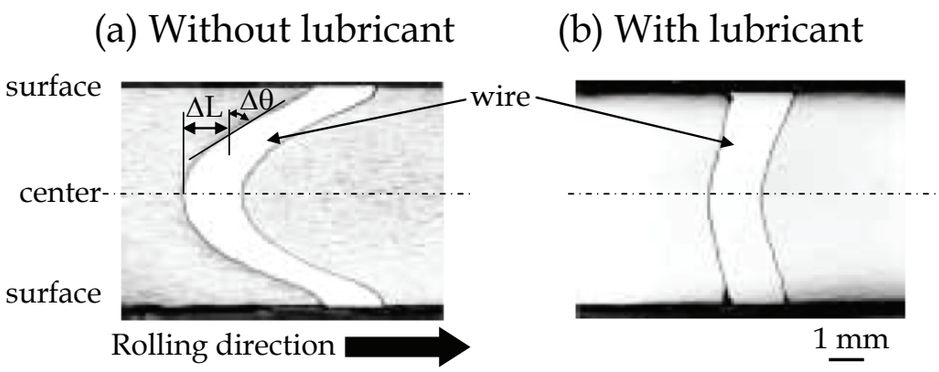

Fig. 3. Flection of stainless wire in sheet after rolling observed by the embedded pin method (Hashimoto et al., 1998). Here, interstitial free steel of 10 mm in initial thickness was rolled by a reduction of 40% per pass at 973 K using a two-high mill with a roll diameter of 300 mm at a rolling speed of 300 mm s^{-1}. The L_d/t_d indicates 3.1 under this rolling condition.

This study aims to exhibit a quantitative correlation between strains and L_d/t_d in metal sheet rolled under various friction coefficients using finite element analysis (FEA), which is a powerful tool for understanding deformation behaviors during a plastic deformation process. The each strain component and equivalent strain at various thickness locations in the sheet during and after rolling were studied in detail, including ΔL and $\Delta\theta$ measured from the embedded-pin method in rolling experiments. Furthermore, the problem associated with universality of the L_d/t_d parameter on the magnitude and distribution of strains is discussed.

2. Finite element model

The elastic-plastic FE simulation was carried out using the FE-code ABAQUS/Explicit ver.6.5-4. A 4-node linear element in a plane strain model, element type CPE4R, was used for sheets of 2 mm and 5.3 mm in initial thickness, t_0, and the rolls were regarded as the rigid body. No remeshing was carried out in the analysis because the deformed mesh by rolling corresponds to the flection of the pin in the embedded-pin method. The Coulomb condition was used as the frictional condition between the rolls and the sheet, $\tau_f = \mu p$, where

τ_f denotes the shear stress, μ is the friction coefficient, and p is the contact pressure. Assuming the Coulomb law, a condition to pull a sheet into rolls bite is given by $\mu > \tan\alpha$, where α denotes the contact angle shown in Fig. 2.

The flection of the pin in the embedded-pin method makes the presence of the shear deformation clear. The pin flection in pure aluminum (Lee et al., 2002), interstitial free (IF) steel (Matsuoka et al., 1997; Sakai et al., 1988; Um et al., 2000; Kamikawa et al., 2007), and Type 304 stainless steel (Zhang et al., 1996; Sakai & Saito, 1999) sheets rolled at various temperatures has been observed using this method. In the present study, the condition of a commercial 1100 Al sheet rolled at ambient temperature without lubricant and without front and back tensions reported by Lee et al., 2002 was referred to as the main rolling condition: initial thickness, t_0=2 mm; nominal reduction per pass, r=50%; roll diameter, d^{ϕ}=255 mm; and rolling speed, 170 mm s^{-1}. The L_d/t_d indicates 7.5 under this rolling condition, and its value becomes smaller with decreasing d^{ϕ}. Nine rolling conditions, Numbers 1-9, employed in the present analysis are listed in Table 1. Numbers 1-6 denote the rolling conditions in which the 1100 Al of t_0=2 mm is rolled by r=50% using a rolling simulator with d^{ϕ}=310, 255, 201, 118, 40, and 15 mm, resulting in L_d/t_d=8.3, 7.5, 6.7, 5.1, 3.0, and 1.8, respectively. In order to study the universality of the L_d/t_d parameter on the strains through sheet thickness, Nos. 7-9 at L_d/t_d = 5.1 are also analyzed under various combinations of t_0, r, and d^{ϕ}. The stress σ–strain ε relationships of the 1100 Al at 301 K employed in the analysis were described by σ=28+105.67 $\varepsilon^{0.32}$ $\dot{\varepsilon}^{0.017}$ MPa depending on the strain rate, $\dot{\varepsilon}$ (Ataka, 2006), and a Young's modulus of 70 GPa and a Poisson's ratio of 0.35 were used as the elastic modulus.

No.	Initial sheet thickness t_0 (mm)	Exit thickness t_1 (mm)	Nominal reduction r (%)	Roll diameter d^{ϕ} (mm)	Projected length L_d (mm)	Average sheet thickness t_d (mm)	Roll bite geometry L_d/t_d	Rolling speed v (mm/s)	Minimum friction coefficient $\mu_{min}=\tan\alpha$
1	2	1	50	310	12.4	1.500	8.3	170	0.08
2				255	11.3		7.5		0.09
3				201	10.0		6.7		0.10
4				118	7.7		5.1		0.13
5				40	4.4		3.0		0.23
6				15	2.7		1.8		0.38
7		1.41	29.5	255	8.7	1.705	5.1		0.07
8		1.76	12	768	9.6	1.880			0.03
9	5.3	2.65	50	310	20.2	3.975			0.13

Table 1. Rolling conditions used in the present study.

In the analysis, the classical metal plasticity models with Mises yield surface, *PLASTIC, HARDENING=ISOTROPIC as keywordin ABAQUS/Explicit, 2006, were employed. The equivalent strain, ε_{eq}, imposed by rolling is defined as follows:

$$\varepsilon_{eq} = \int_0^{t(steady)} \frac{d\varepsilon_{eq}}{dt} dt \tag{1}$$

where $d\varepsilon_{eq}/dt$ denotes the incremental equivalent strain, and $t_{(steady)}$ is the rolling time. Since an incremental strain in the x direction, $d\varepsilon_{xx}/dt$, is equal to a minus incremental strain in the y direction, $-d\varepsilon_{yy}/dt$, under the plane strain condition, the incremental equivalent strain, i.e., the equivalent strain rate, $d\varepsilon_{eq}/dt$, is represented as below:

$$\frac{d\varepsilon_{eq}}{dt} = \frac{2}{\sqrt{3}}\sqrt{\left(\frac{d\varepsilon_{xx}}{dt}\right)^2 + \frac{1}{4}\left(\frac{d\gamma_{xy}}{dt}\right)^2} \tag{2}$$

In equation (2), $d\gamma_{xy}/dt$ is the incremental shear strain. Since the direction of the shear stress, τ_f, in a roll bite changes to opposite directions before and after a neutral plane NP, shown in Fig. 2, the total shear strain, γ, must be expressed as follows:

$$\gamma = \int_0^{t(NP)} \frac{d\gamma_{xy}}{dt} dt + \int_{t(NP)}^{t(steady)} \left|\frac{d\gamma_{xy}}{dt}\right| dt \tag{3}$$

Here, the first term in the above equation denotes a positive shear strain, $\gamma+$, induced by the shear stress, τ_f, before NP, and the second term is the negative shear strain, $\gamma-$, by the τ_f after NP. In other words, the γ represents the total magnitude of the shear strain γ_{xy} taking into account the deformation history during rolling. At the thickness center with no shear deformation, the $d\gamma_{xy}/dt$ is always zero, and the $d\varepsilon_{xx}/dt$ is constant throughout rolling. Hence, ε_{eq} at the center agrees with the value $2/\sqrt{3}$ ln{1/(1−r)} calculated simply from a reduction in thickness independent of the deformation history, where $\varepsilon_{xx} = -\varepsilon_{yy} = \ln\{1/(1-r)\}$ and $\gamma = 0$.

3. Simulation results

3.1 Mesh dependence of strain in rolled sheet

At first, the appropriate mesh division in the FEA was examined because the magnitude of strain depends certainly on mesh size. Figure 4 shows the variation of the equivalent stain, ε_{eq}, at a surface against the initial element length in the thickness direction, t_{el}, for FEA using μ=0.3 under the rolling condition No. 2 in Table 1, where the initial element length in the rolling direction, L_{el} , is 0.0231 mm. The figure inset describes the FE mesh near the sheet surface. It is found that ε_{eq} at the surface depends strongly on the t_{el} as expected. The ε_{eq} increases with decreasing t_{el} and tends to be almost constant at t_{el} below 0.03 mm. On the other hand, ε_{eq} at the thickness center exhibited about 0.80 regardless of t_{el} below 0.26 mm. This magnitude corresponds to a value, $2/\sqrt{3}$ ln{1/(1−r)}, of equivalent strain calculated theoretically under the plane strain condition, where the reduction r is 0.5 in the present condition. In the present analysis, the sheet thickness was divided into 66 elements, i.e., t_{el}=0.03 mm was used throughout the sheet. Moreover, the sheet length was determined through some simulations on a steady-state of deformation where the strains remains constant along the RD. As a result, the finite element mesh in the sheet with dimensions of 2 mm^t×15 mm^L included 20167 nodes and 19800 elements as illustrated in Fig. 5. Here, a minimum L_{el} is 0.0231 mm at the mid-length (center element), and L_{el} gradually increases toward the front and back from the center. The L_{el} at the front and back edges of the sheet is the same 0.0923 mm. Similar, for the rolling condition No. 9 of t_0=5.3 mm in Table 1, t_{el}=0.03 mm was used throughout the sheet. Thus, the finite element mesh in the sheet with dimensions of 5.3 mm^t×15 mm^L included 26488 nodes and 26100 elements.

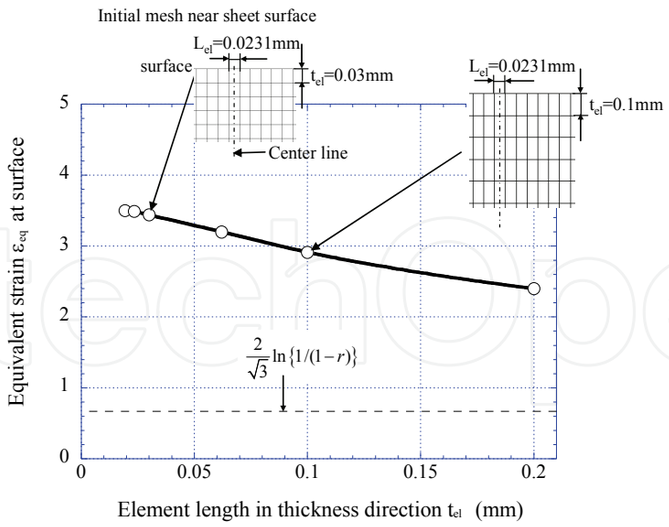

Fig. 4. Variation of ε_{eq} at surface in the rolled Al with μ=0.3 against initial element length in thickness direction. Here, rolling condition No.2 in Table 2 was used.

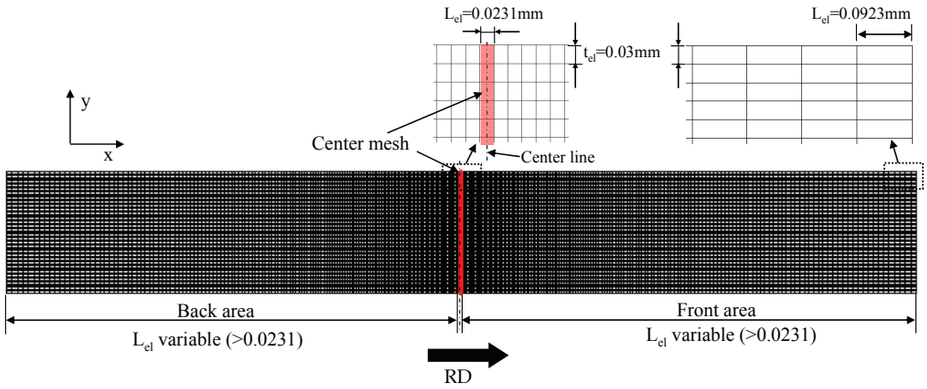

Fig. 5. Initial finite element mesh used in the analysis. Here, L_{el} denotes the mesh length in rolling direction (RD).

3.2 Variations of ΔLs, Δθs, and ε_{eq} at the sheet surface with roll bite geometry

Figure 6 shows the effect of the L_d/t_d ratio on the distance from center to surface in RD, ΔLs, the angle of inclination from the y axis, Δθs, and the equivalent stain, ε_{eq}, at the surface of a 50% rolled Al sheet in the friction coefficient range of $\tan\alpha \le \mu \le 0.4$. The slip areas in Fig. 6 denote a condition of $\mu < \tan\alpha$ on the basis of the Coulomb law, and the open symbol in Fig. 6(a) represents the observed result, ΔLs = 1.1, of the pin method reported by Lee et al., 2002. Although the ΔLs have no large difference by L_d/t_d under a low friction of $\mu \le 0.2$, this difference becomes larger with increasing L_d/t_d under high friction. Similarly, in Fig. 6(b), the Δθs becomes larger with increasing L_d/t_d and μ. However, under L_d/t_d = 8.3 of the largest roll bite geometry in the present study, the Δθs decreases from μ= 0.35 to 0.4.

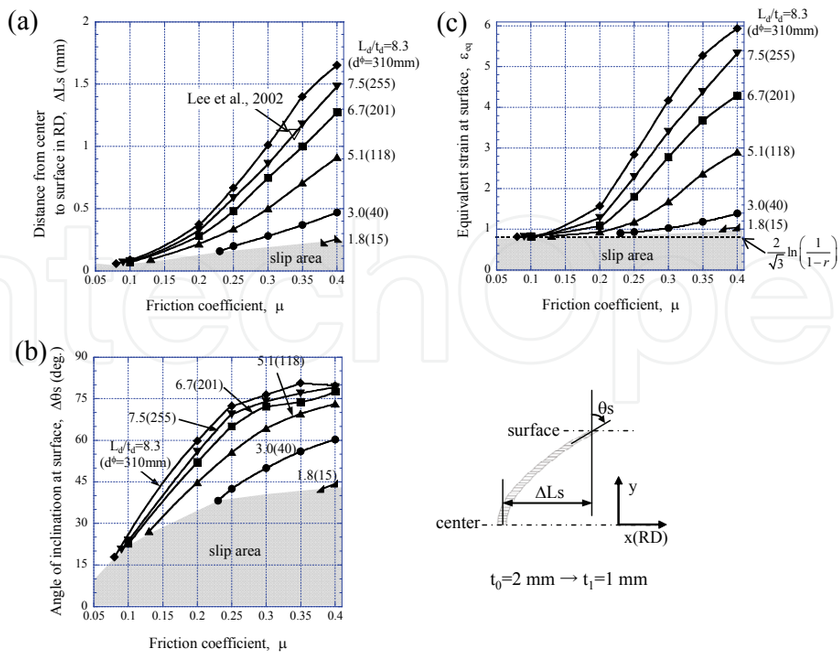

Fig. 6. (a) ΔLs, (b) Δθs, and (c) ε_{eq} at the surface of a 50% rolled Al sheet against μ under different roll bite geometries L_d/t_d (Nos.1-6 shown in Table 1).

Furthermore, the Δθs indicates a large value of 45° at μ= 0.4 even if the roll bite geometry is very small, L_d/t_d =1.8. The ε_{eq} increases with increasing L_d/t_d under the same μ. Although the tendency is slight under $\mu \leq 0.2$, it becomes remarkable under $\mu > 0.2$ at $L_d/t_d \geq 5.1$. At μ= 0.4 of a high friction condition, the ε_{eq} exhibits a very large value of 6.0, which is seven times higher than that at the center, $2/\sqrt{3}\ \ln\{1/(1-r)\}$, under $L_d/t_d = 8.3$. On the other hand, under L_d/t_d = 1.8 the ε_{eq} is 1.0, which is slightly higher than that at the center. The variation of ε_{eq} at the sheet surface as functions of μ and L_d/t_d is very similar to that of ΔLs. Using Fig. 6(a,c), it is considered that the friction coefficient was μ=~0.34 in the rolling experiment under L_d/t_d = 7.5 reported by Lee et al., 2002 and the ε_{eq} of 4.23, which is five times higher than that at the center, was introduced to the sheet surface. Kamikawa et al., 2007 reported that the microstructural parameters, fraction of high-angle grain boundaries and average misorientation, at the surface in the IF steel processed by one ARB cycle at 773K without lubricant correspond to those at the center in the IF steel processed by five ARB cycles with lubricant. The FE result shown in Fig. 6 is consistent with their microstructural results, although a material is different. The results of Fig. 6(c) indicate that the ε_{eq} introduced to the sheet surface by rolling under the unlubricated condition is significantly different by the roll diameter even if the initial thickness, nominal reduction, and friction condition are the same. It is clear that ε_{eq} at the surface depends on not only the friction condition between the rolls and the sheet but also the roll bite geometry. It is evident from Fig. 6(b,c) that the ε_{eq} and Δθs at the surface after rolling with μ=0.4 under L_d/t_d = 5.1 agree with those with μ=0.25 under L_d/t_d = 8.3. However, in Fig. 6(a) the value of ΔLs does not agree at these conditions. Furthermore, although the Δθs for μ=0.4 under $L_d/t_d \geq 6.7$ indicates almost the same value,

the ΔLs and ε_{eq} are different under these conditions. These differences are attributed to the complicated deformation history near the surface, as described in Subsections 3.3.3 below.

3.3 Deformation behavior at various thickness locations in a rolled sheet

3.3.1 Flection of pin after rolling

Figure 7 shows deformed meshes of a center part of the FE mesh (center mesh in Fig. 5) after rolling with different μ, corresponding to the pin described in Fig. 2. Here, the rolling condition No.2 in Table 1 was used. The flection through the thickness becomes larger with increasing μ. This feature is consistent with the experimental results in which the flection of the embedded pin is larger in a sheet rolled without lubricant than that with lubricant, as shown in Fig. 3. Although the shear strain and equivalent strain are always calculated from the inclination of the pin, based on equations proposed by Sakai et al., 1988, the embedded-pin method does not exhibit the exact value of strains, because these equations are derived under three assumptions; I) The ratio of incremental shear strain to incremental compressive strain is constant during rolling; II) The incremental compressive strain is uniform through the thickness; III) Plane strain conditions prevail in the deformation zone. And, the effect of reverse shear deformation after the neutral plane, NP, shown in Fig. 2, is not considered in these assumptions. As a result, it is clarified from strain histories during rolling shown in Fig. 9 below that two assumptions I) and II) are not proper.

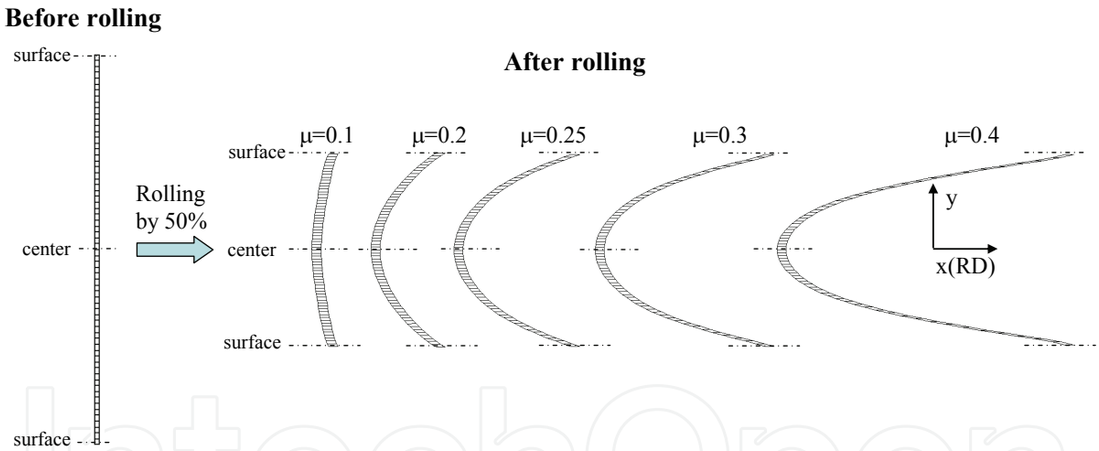

Fig. 7. Initial mesh and deformed mesh after rolling with various friction coefficients μ under rolling condition No.2 in Table 1.

3.3.2 Variations of ΔL and Δθ through sheet thickness after rolling

Figure 8 shows the distributions of the distance from the center in RD, ΔL, and the angle of inclination from the y axis, Δθ, through the sheet thickness after rolling with various μ under L_d/t_d =7.5 (d^{ϕ}=255 mm) and L_d/t_d = 5.1 (d^{ϕ}=118 mm), respectively. Here, these data were obtained from the values of the integration point for each element divided into 33 through the sheet thickness. In Fig. 8(a), the ΔL increases with increasing μ throughout thickness locations, becomes gradually larger toward the surface from the center, and takes a maximum at the surface. For the same μ, the ΔL under L_d/t_d =7.5 is larger than that under L_d/t_d = 5.1 throughout thickness locations. In Fig. 8(b), the Δθ similarly increases with

increasing μ, but the distributions of Δθ through thickness are different by μ. Under L_d/t_d =7.5, the Δθ for μ = 0.1 slightly increases from y=0 (center) to 0.45 and there is a steep increase toward the surface thereafter. The Δθ for μ = 0.2 monotonously increases toward the surface. The Δθ for μ ≥ 0.25 increases with the distance y, takes a maximum at a thickness location near the surface, and decreases toward the surface from the location. The feature can be seen clearly in the flection of pin embedded in IF-steel sheets rolled at 973 K under the unlubricated condition, as shown in Fig. 3 (Matsuoka et al., 1997; Hashimoto et al., 1998; Kawabe et al., 1996). The location where the Δθ takes a maximum is slightly away from the surface with increasing μ. The distributions of Δθ for μ = 0.2 and 0.4 under L_d/t_d =5.1 are similar to those for μ = 0.1 and μ ≥ 0.25 under L_d/t_d = 7.5. Furthermore, the magnitude of Δθ near the surface for μ = 0.4 under L_d/t_d =5.1 agrees with that for μ = 0.3 under L_d/t_d = 7.5. At this time, the γ at the surface for these conditions was almost the same value of ~ 4.7, but the ε_{eq} was different, where ε_{eq} =3.4 for μ = 0.3 under L_d/t_d = 7.5 and ε_{eq} =2.9 for μ = 0.4 under L_d/t_d =5.1 (Fig. 6(c)).

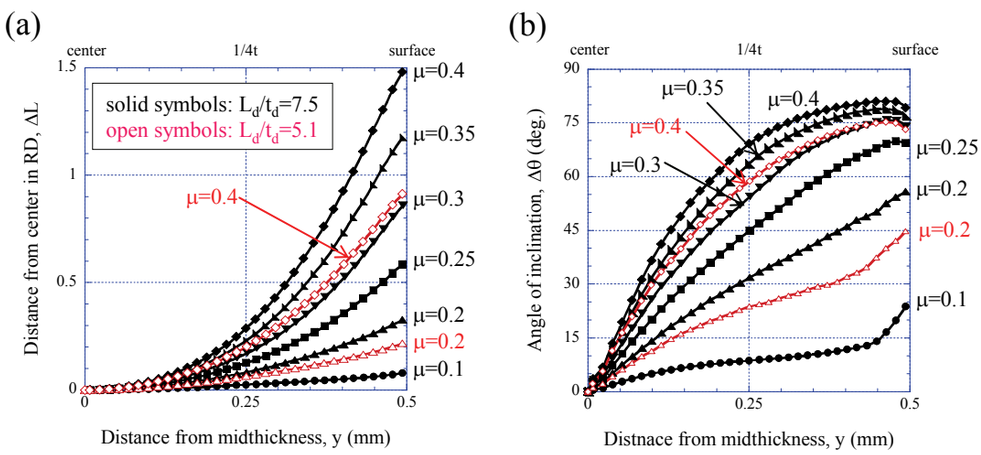

Fig. 8. Variations of (a) ΔL and (b) Δθ through sheet thickness after rolling with friction coefficient μ under L_d/t_d =7.5 (No. 2 in Table 1) and L_d/t_d =5.1 (No. 4 in Table 1).

3.3.3 Strain histories during rolling

The histories of the total strain in the x direction, ε_{xx}, the total shear strain, γ, and the equivalent strain, ε_{eq}, at five elements, i.e., e1, e4, e7, e17 and e33, through sheet thickness during rolling with μ= 0.4 under L_d/t_d = 7.5 are shown in Fig. 9, including deformed meshes at times of 0.0875, 0.1, and 0.14 s illustrated in the inset. Here, the NP denotes the time at which the shear stress τ_f for each element equals zero and the stress in the y direction becomes a maximum (Underwood, 1952). The e1 corresponds to the element located in the sheet surface, e4, to the element for which the Δθ indicated a maximum value for μ = 0.4 (Fig. 8(b)), e33, to the element located in the center, e17, to the element at 1/4 thickness located between e1 and e33, and e7, to the element between e4 and e17. From Fig. 9, all strains at e17 monotonously increase with increasing time. This means that each strain rate, $d\varepsilon_{xx}/dt$, $d\gamma/dt$, and $d\varepsilon_{eq}/dt$, at thickness locations from the center to the 1/4 thickness is almost constant during rolling. Furthermore, the strain rates at e17 increases as a result of

the shear deformation more than that at e33 without γ. Hence, the ε_{eq} at the 1/4 thickness (e17) becomes larger than that at the center (e33) which agrees with the value $2/\sqrt{3}$ ln{1/(1−r)} calculated simply from reduction in thickness due to γ=0 constantly. On the other hand, all strain rates at e7, e4, and e1 near the surface vary during rolling by the γ effect, and the ε_{xx} and ε_{eq} increase as a thickness location approaches the surface (Fig. 9(a,c)). However, the γ at e4 corresponding to the thickness location for which the Δθ indicated a maximum value in Fig. 8(b) is smaller than that at e7 (Fig. 9(b)). The shear strain rate, dγ/dt, at e4 is initially faster than that at e7, but the γ indicates the same value, γ+= ~2.9, before the NP, because the time of dγ/dt≈0 during rolling is longer in e4 than in e7. After the NP, the dγ/dt at e7 inversely becomes faster than that at e4. Namely, although the positive shear strain, γ+, is the same at these two locations, the negative shear strain, γ−, at e4 is smaller than that at e7.

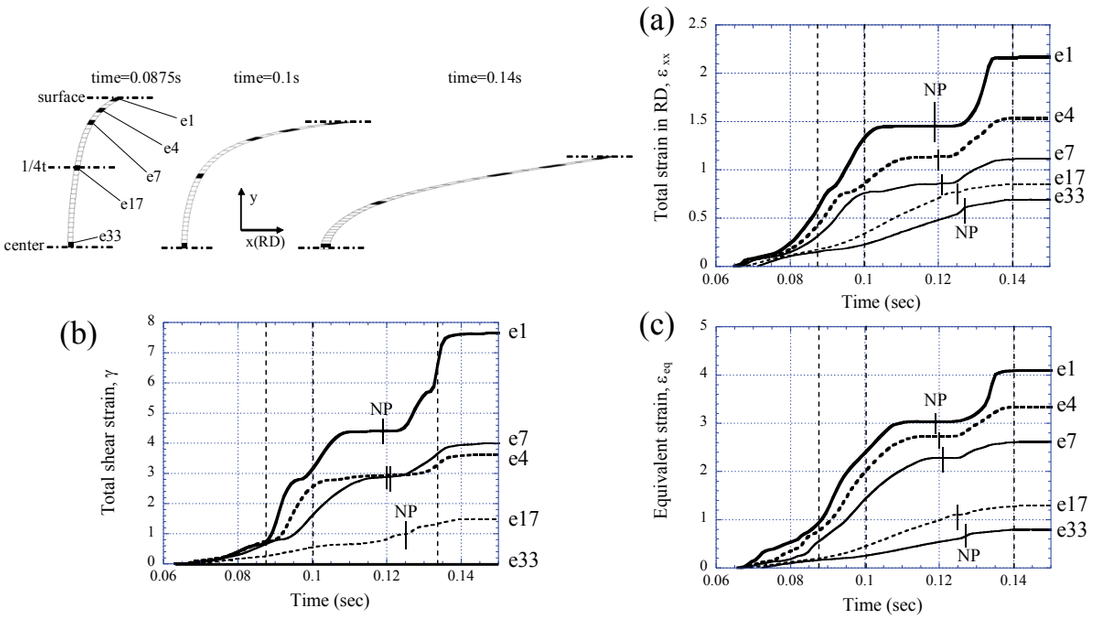

Fig. 9. Histories of (a) ε_{xx}, (b) γ, and (c) ε_{eq} at five thickness locations (as inset) during rolling with μ=0.4 under L_d/t_d=7.5 (No. 2 in Table 1).

Such shear strain history was not seen in 0.13 ≤ μ ≤ 0.4 under L_d/t_d = 5.1 (d^{ϕ}=118 mm). This feature is further exhibited in Fig. 10, where the variations of γ, γ+, and γ− through thickness are shown. Here, the thickness locations corresponding to five elements illustrated in the inset of Fig. 9 are displayed. In Fig. 10(a), the γ+ initially increases with the distance y. Its incremental rate becomes larger from e17 (y=0.25) to e7 (y=0.4), becomes constant until e4 (y=0.45) thereafter, and shows a steep increase from e4 to e1 (y=0.5). On the other hand, the γ gradually increases from e33 (y=0) to e7 (y=0.4), decreases from e7 to e4 (y=0.45), and shows a sharp increase thereafter. The magnitude of γ− is smaller than that of γ+ throughout thickness locations. As a result, the γ which expresses these sums shows a distribution with a sudden dip at y=0.45 near the surface, where the Δθ indicated a

maximum value (Fig. 8(b)). Although a similar variation of $\Delta\theta$ with a maximum was seen in $\mu = 0.4$ under $L_d/t_d = 5.1$, the γ distribution with the sudden dip in Fig. 10(a) does not appear in Fig. 10(b), where the variations of γ, $\gamma+$, and $\gamma-$ through thickness after rolling with $\mu = 0.4$ under $L_d/t_d = 5.1$ are shown. In Fig. 10(b), the magnitude of $\gamma-$ is smaller than that of $\gamma+$ throughout thickness locations except the surface, and the $\gamma-$ exhibits the same magnitude as the $\gamma+$ at the surface. The feature which $\gamma+$ equals $\gamma-$ at the surface was the same in the friction coefficient range of $0.13 \le \mu \le 0.4$ under $L_d/t_d = 5.1$. This feature was also observed in $0.1 \le \mu \le 0.3$ under $L_d/t_d = 7.5$, as shown in Fig. 6(b) of T.Inoue & N.Tsuji, 2009. Consequently, the magnitude of the shear strain $\gamma+$ before the NP is larger than that of the reverse shear strain $\gamma-$ after the NP through thickness, but these magnitudes exhibit the same value at the sheet surface. Provided that a sheet is rolled with a high friction condition under a large roll bite geometry, the magnitude of $\gamma+$ becomes larger than that of $\gamma-$ throughout thickness due to the sudden dip of $\gamma-$ near the surface.

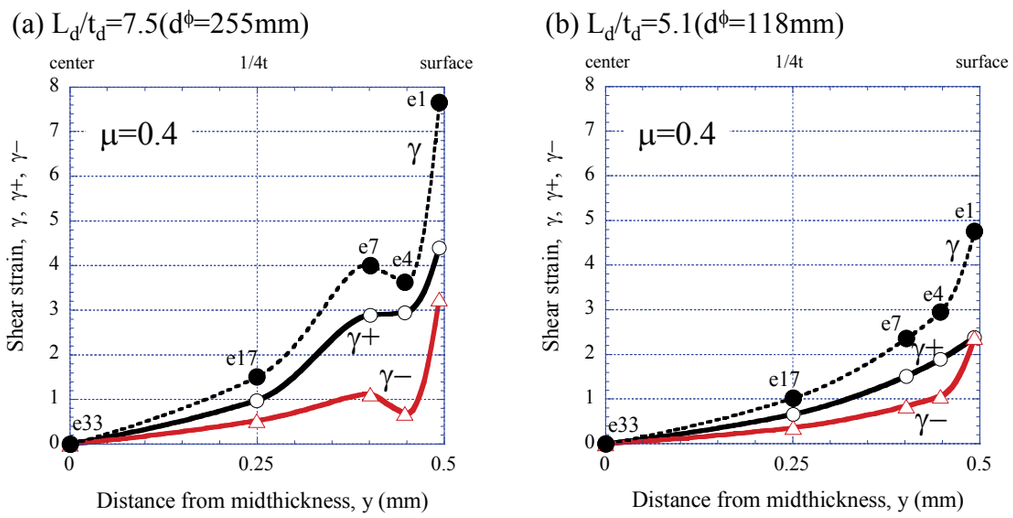

Fig. 10. Variations of the total shear strain γ , positive shear stain $\gamma+$, and reverse shear strain $\gamma-$ through sheet thickness after rolling with μ=0.4. Here, e1, e4, e7, e17 and e33 are displayed in the inset of Fig. 9.

3.4 Strain distributions through sheet thickness after rolling

According to the embedded-pin method (Sakai et al., 1988; Matsuoka et al., 1997), the "apparent" shear strain, $\gamma_{(pin)}$, shows a maximum at the thickness location of 0.1~0.2 from surface, and, hence, the "apparent" equivalent strain, $\varepsilon_{eq(pin)}$, also takes the maximum there. Here, in Sakai et al., 1988, a large roll bite geometry of 9.1 had been empoyed. This is clear from the variation of $\Delta\theta$ through sheet thickness in Fig. 8(b). The $\gamma_{(pin)}$ is calculated from the inclination of the pin after rolling. Provided the direction of shear deformation remains unchanged during rolling, the $\gamma_{(pin)}$ and $\varepsilon_{eq(pin)}$ must take their maximum at the surface. However, since the direction of shear deformation changes to the opposite direction at the NP, the inclination of mesh at the surface becomes smaller in the surface layer under high friction and large roll bite geometry conditions, as shown in Fig. 8(b). Therefore, the $\varepsilon_{eq(pin)}$

measured by the embedded-pin method would be underestimated in the surface layer compared with the "substantial" equivalent strain obtained in the present study.

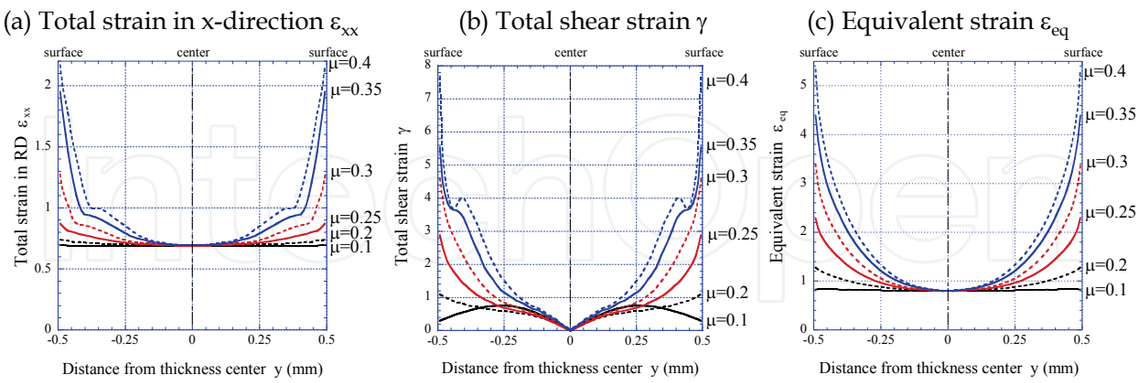

Fig. 11. Distributions of ε_{xx}, γ, and ε_{eq}, through sheet thickness for various friction coefficients μ under L_d/t_d =7.5 (No. 2 in Table 1).

Figure 11 represents the distributions of the "substantial" γ and ε_{eq} through the sheet thickness after rolling with various μ under the rolling condition No. 2 in Table 1. Similarly, the distribution of ε_{xx} (= $-\varepsilon_{yy}$) is shown in Fig. 11 because all the strains are associated as shown in Fig. 9. The γ at the thickness center is always zero in Fig. 11(b). The γ for μ=0.1 takes a maximum at y=±0.25mm (1/4t) and decreases toward the surface thereafter. It is likely that this distribution results from the roll bite geometry L_d/t_d, because the corresponding strain ε_{xx} is constant through the sheet thickness as shown in Fig. 11(a). The ε_{xx} for friction coefficient other than μ=0.1 gradually increases toward the surface from the center, but for μ=0.35 and 0.4 there is a sharp raise at the thickness location of 0.05~0.15 from surface. In Fig. 11(b), γ for μ=0.2 to 0.3 increases toward the surface from the center. However, the distributions of γ for $\mu \geq 0.35$ are different from those for μ=0.2 to 0.3. Especially for μ=0.4 there is a sudden dip at the thickness location near surface. It is considered that this behavior is attributed to the decrease in the reverse shear strain $\gamma-$ as shown in Fig. 10(a). If the $\gamma+$ and $\gamma-$ are the same magnitude regardless of the change in μ, the total shear strain γ might gradually increase toward the surface from the center such as γ for μ=0.2 to 0.3, and, furthermore, larger total shear strain might occur at the surface. On the other hand, in Fig. 11(c), ε_{eq} at the thickness center is constant regardless of μ, and its magnitude indicates 0.80 because no shear strain is imposed at the center. Although ε_{eq} for μ=0.1 looks almost constant throughout the thickness, the ε_{eq} showed a distribution in the strain range of $0.8 \leq \varepsilon_{eq} \leq 0.83$; it increases toward the surface from zero (y=0) at the center, takes a maximum at $y \approx \pm 0.45$ mm, and decreases thereafter. It is considered that this distribution is the effect of L_d/t_d. The ε_{eq} for all other μ gradually increases toward the surface from the center and shows a distribution with the maximum at the surface. The maximum ε_{eq} increases with increasing μ, and ε_{eq} for μ=0.4 reaches 5.33, which is six times higher than that at the center. The ε_{eq}=5.33 corresponds to a 99% reduction in plane strain compression. In the distribution of ε_{eq}, a sharp raise or a sudden dip, as seen near the surface of ε_{xx} and γ are not observed. This means that the equivalent strain ε_{eq} that denotes

scalar amount varies continuously throughout sheet thickness regardless of the roll bite geometry and the friction between the rolls and the material surface. On the other hand, strains in each component that denote vector amount vary complicatedly in the sheet thickness. Hence, it is found that a much larger ε_{eq} can be introduced to the sheet surface through a complicated deformation by the shear strain effect.

3.5 Strain distributions in ARB

There are numerous reports on microstructure evolution in various sheet materials by ARB process (Hidalgo et al., 2010; Kolahi et al., 2009; Xing et al., 2002). In most papers, a rolling by a 50% reduction in thickness is conducted without lubricant, and equivalent strain calculated simply from reduction in thickness has been used regardless of a high friction condition. However, it is found from previous results that equivalent strain introduced in a rolled sheet is different by the effects of not only friction condition but also roll diameter used.

From Figs. 6(a,c) and 11(b,c), γ and ε_{eq} at the surface imposed by the first cycle of ARB at ambient temperature reported by Lee et al., 2002 show the values of 5.60 and 4.23, respectively. That is, a much larger equivalent strain, which is five times higher than that at the center, is introduced to the surface. Here, it is considered that the friction coefficient is $\mu \approx \sim 0.34$. Moreover, assuming that the same deformation is repeated in the following cycles, γ and ε_{eq} at the surface in the multi-cycle ARB-processed 1100 Al can be estimated by γ=5.60 N and ε_{eq} =4.23 N, respectively, where N denotes the number of cycles. On the other hand, the γ and ε_{eq} at the center are calculated by γ=5.60 (N–1) and ε_{eq}=0.8+4.23 (N–1), respectively. Utsunomiya et al., 1999 showed the flection of the pin in the 1100 Al processed by one ARB cycle at 473 K with and without lubricant under the same roll bite geometry as Lee et al., 2002. Here, ΔLs indicated ~0.15 with lubricant and ~1.5 without it. Since the effect of temperature in the rolled Al or IF steel sheet on the relation among ε_{eq}, γ, and ΔLs is small in comparison with the friction effect (Um et al., 2000; Inoue & Tsuji, 2009), it is likely from Figs. 6(a,c) and 11(b,c) that the strain at the surface is $\gamma \approx 0.59$ and $\varepsilon_{eq} \approx 0.97$ for rolling with lubricant and $\gamma \approx 7.66$ and $\varepsilon_{eq} \approx 5.34$ for rolling without it. Here, it is considered that the friction coefficient is about ~0.12 for rolling with lubricant and ~0.40 for rolling without it. That is, equivalent strain and shear strain at the surface in a sheet rolled without lubricant are five times and twelve times higher than the strains with it. Namely, ε_{eq} at the surface in the 1100 Al processed by one ARB cycle without lubricant would correspond to ε_{eq} in that processed by five ARB cycles with lubricant. Consequently, since ARB process shown in Fig. 1(b) is usually conducted by a 50% reduction of thickness without lubricant to aid bonding, a rolling condition with large roll bite geometry is desirable for fabricating ultrafine-gained materials efficiently.

3.6 Variations of the total shear strain γ and equivalent strain ε_{eq} against ΔL or $\Delta\theta$

The embedded-pin method has a limitation on the quantification of strains imposed by rolling, as mentioned previously. In particular, the strains near the surface are determined by very complicated histories during rolling, as shown in Fig. 9. However, if the magnitude and distribution of strains in a rolled sheet can be quantitatively estimated by using experimental measurements, such as ΔL or $\Delta\theta$ observed from the pin flection shown in Fig. 3, these quantitative strain analyses would be useful for designing the microstructure of the

sheet metal by rolling. Figure 12(a,b) shows the variations of γ and ε_{eq} with ΔL through sheet thickness for different values of μ under L_d/t_d =7.5 and Fig. 12(c,d) shows the variations of γ and ε_{eq} with $\Delta\theta$. Here, all data were obtained from the values of the integration point for 33 elements in sheet thickness, as shown in Fig. 8. The $\Delta L = 0$ and $\Delta\theta = 0$ correspond to a location of the thickness center.

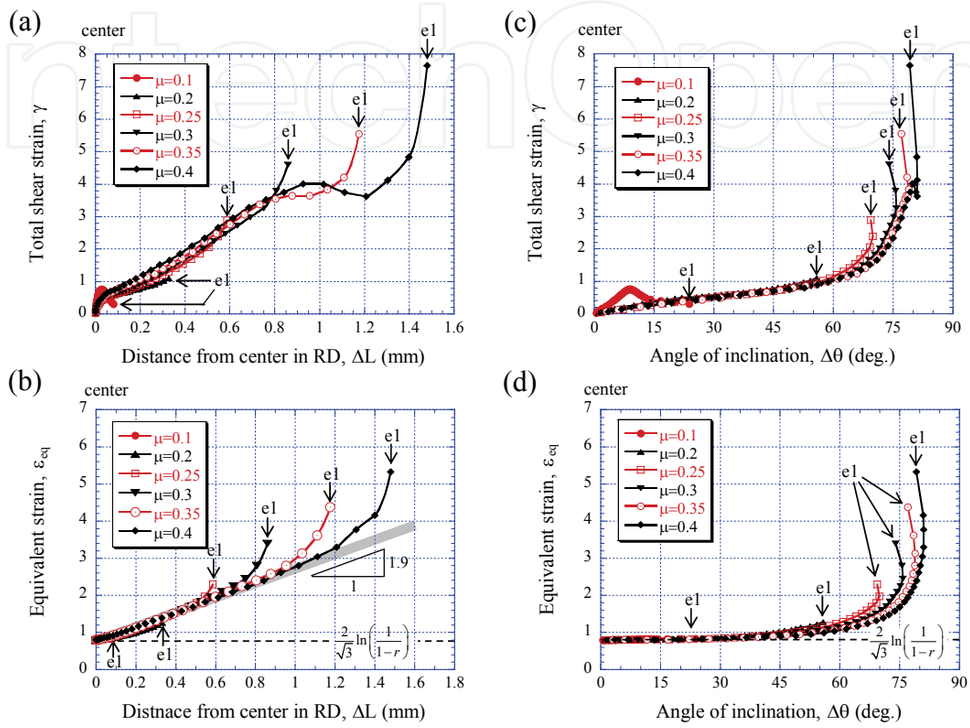

Fig. 12. Variations of (a) γ and (b) ε_{eq} with ΔL and (c) γ and (d) ε_{eq} with $\Delta\theta$ through thickness in 50% rolled Al for various friction coefficients μ under L_d/t_d =7.5 (No. 2 in Table 1). Here, e1 denotes data at the sheet surface shown in the inset of Fig. 9.

In Fig. 12(a,c), the $\gamma - \Delta L$ and $\gamma - \Delta\theta$ relations for $\mu = 0.1$ are significantly different from the relations for other μ. The γ for the μ close to tan α, which is a condition to pull a sheet into the roll bite, took a maximum at $y \approx \pm 0.25$ mm (1/4 thickness) and decreased toward the surface thereafter, as shown in Fig. 11(b). This is because the distribution of γ is dominated by the roll bite geometry L_d/t_d due to the small effect of μ. The γ for $\mu \geq 0.2$ increases as the ΔL or $\Delta\theta$ becomes larger, i.e., the thickness location approaches a sheet surface. However, since there is a decrease of the negative shear strain $\gamma-$ near the surface, as shown in Fig. 10(a), the γ for $\mu \geq 0.35$ initially increases with increasing the ΔL or $\Delta\theta$, decreases near the surface, and shows a steep increase thereafter. The $\gamma - \Delta\theta$ relations, except $\mu = 0.1$, have a good correlation, compared to the $\gamma - \Delta L$ relation. In particular, the variation of γ with $\Delta\theta$ until 60° is almost the same despite μ. It is likely that the $\Delta\theta$ depends strongly on the shear deformation. It is evident from Fig. 12(b,d) that the ε_{eq}, including all strain components as defined in equation (2), has very good correlation with the ΔL and $\Delta\theta$. The ε_{eq} monotonically increases with increasing the ΔL, and the relation is expressed by $\varepsilon_{eq} = 1.9\ \Delta L$

+ 0.8, but the ε_{eq} sharply increases near the surface by the effect of the shear strain (Fig. 12(b)). On the other hand, in Fig. 12(d), the ε_{eq} remains 0.8 calculated by $2/\sqrt{3}\ \ln\{1/(1-r)\}$ in the range of $0 \le \Delta\theta \le 30°$, slightly increases with $\Delta\theta$ thereafter, and sharply increases at $\Delta\theta \ge 70°$ by the shear deformation effect. It is clear from Fig. 12 that the ε_{eq} has better correlation with the ΔL and $\Delta\theta$, than γ. This means that ΔL and $\Delta\theta$ are determined by a combination of the strains in the x and y directions and the shear strain and their histories during rolling. As shown in Figs. 6 and 8, the deformation behaviors in a rolled sheet depend strongly on not only the friction but also the roll bite geometry, especially when rolling with high friction. Figure 13 shows the variations of ε_{eq} with ΔL and $\Delta\theta$, respectively, in a 50% rolled Al with μ=0.4 under various L_d/t_d of five rolling conditions, Nos. 1-5, in Table 1. These correlations agree with the ε_{eq} –ΔL and ε_{eq} –$\Delta\theta$ relations shown in Fig. 12(b,d). Consequently, the L_d/t_d ratio has a similar effect on μ regarding the relation among ε_{eq}, ΔL, and $\Delta\theta$ through sheet thickness after rolling.

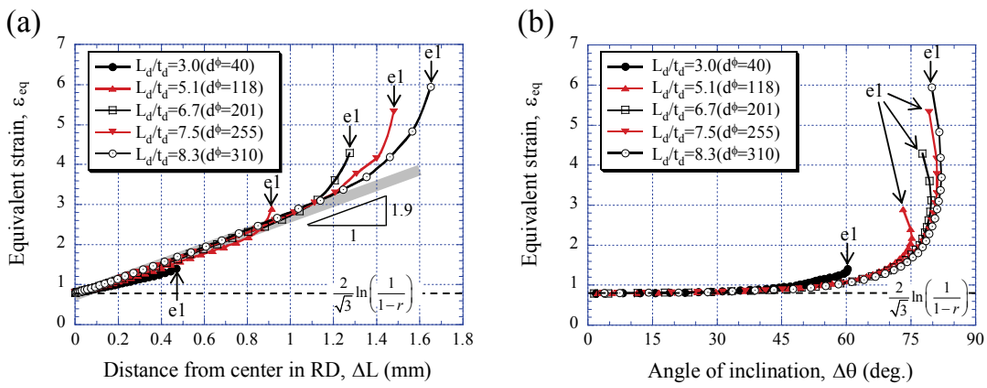

Fig. 13. Variations of ε_{eq} with (a) ΔL and (b) $\Delta\theta$ through thickness in 50% rolled Al with μ =0.4 under various L_d/t_d (Nos. 1-5 in Table 1). Here, e1 denotes data at the surface shown in the inset of Fig. 9.

3.7 Universality of the roll bite geometry on strains through thickness in a rolled sheet

As a condition to impose a large equivalent strain by rolling, the roll bite geometry is as important a processing parameter as the friction condition. The roll bite geometry L_d/t_d is determined by the thickness before and after rolling, t_0 and t_1, and the roll diameter, d^ϕ, as shown in Fig. 2. However, even if the L_d/t_d is the same value, the deformation behaviors through sheet thickness may be different by a combination of t_0, t_1, and d^ϕ because the deformation histories during rolling are very complicated under high friction conditions. Figure 14 shows the distributions of $\Delta\theta$ and equivalent strain added by the shear deformation, $\varepsilon_{eq(shear)}$, through thickness in the rolled Al with μ=0.3 under the rolling conditions Nos. 4, 7-9 of L_d/t_d = 5.1 in Table 1. Here, the horizontal axis was normalized by the half of sheet thickness after rolling, i.e., $2y/t_1$ = 0, ±0.5, and ±1 indicate the center, 1/4 thickness, and surface, respectively, in the sheet. The $\varepsilon_{eq(shear)}$ represents the equivalent strain added by shear deformation as defined by $\varepsilon_{eq} - 2/\sqrt{3}\ \ln\{1/(1-r)\}$ and equals zero at the center of γ=0. It is found from Fig. 14(a) that, for all conditions, the $\Delta\theta$ through thickness

does not exhibit exactly the same distribution and magnitude. In particular, the magnitudes for Nos. 4 and 9 at the same r are significantly different from those for Nos. 7 and 8.

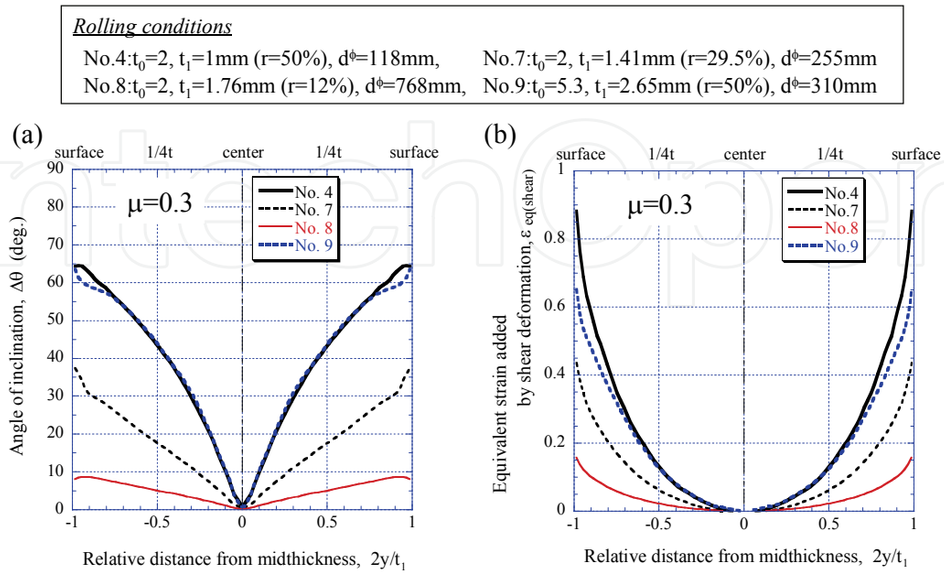

Fig. 14. Distributions of (a) Δθ and (b) equivalent strain added by shear deformation, $\varepsilon_{eq(shear)}$, through sheet thickness in rolled Al with μ=0.3 under L_d/t_d=5.1. Here, full details of the rolling conditions are shown in Table 1.

Numbers 4 and 9 indicate the same magnitude at all thickness locations except near $y/t_1 = \pm 0.9$. The magnitude of Δθ decreases with decreasing r under the same t_0 (Nos. 4, 7, 8). The friction coefficient range of $0.13 \le \mu \le 0.4$ showed a similar feature. This result indicates that the Δθ measured from the embedded-pin method is different by r even if the L_d/t_d has the same value under the same t_0. Therefore, we should use a reduction of the thickness, r, as a variable of the L_d/t_d. In Fig. 14(b), the $\varepsilon_{eq(shear)}$ also exhibits the same tendency. At the surface, the $\varepsilon_{eq(shear)}$ for No. 4 of r=50% is 0.88, which is twice as high as that for No. 7 of r=29.5% and five times higher than that for No. 8 of r=12%. These values are similar to the relations of the equivalent strain calculated simply from the r, i.e., ε_{eq} at the center; ε_{eq} = 0.8, 0.4, 0.15 for r=50%, 29.5%, 12%, respectively. Furthermore, although the Δθ at the surface in Nos. 4 and 9 indicated the same value in Fig. 14(a), the $\varepsilon_{eq(shear)}$ is larger in No. 4 than in No. 9. This feature was the same in the range of $\mu \ge 0.3$, and the difference of $\varepsilon_{eq(shear)}$ at the surface increased with increasing μ. However, the $\varepsilon_{eq(shear)}$ at the surface in the Nos. 4 and 9 indicated the same magnitude in the range of $\mu \le 0.25$. On the other hand, the $\varepsilon_{eq(shear)}$ from the center to the 1/4 thickness in No. 4 is in good agreement with that in No. 9 (Fig. 14(b)). A similar feature was seen in the friction coefficient range of $0.13 \le \mu \le 0.4$. As shown in Fig. 9, at thickness locations from the center (e33) to the 1/4 thickness (e17), the strain rates are almost constant during rolling. In other words, the magnitude of $\varepsilon_{eq(shear)}$ at the thickness locations which take a constant strain rate during rolling agrees under the L_d/t_d ratio with the same r. However, the $\varepsilon_{eq(shear)}$ from the 1/4 thickness to the surface is not the same magnitude in the range of $\mu \ge 0.3$, and the $\varepsilon_{eq(shear)}$ at the locations becomes larger with

decreasing t_0 for the same r. Figure 15 shows the distributions of $\Delta\theta$ ($-1 \le 2y/t_1 \le 0$) and $\varepsilon_{eq(shear)}$ ($0 \le 2y/t_1 \le 1$) for μ=0.25. It can be seen that the $\varepsilon_{eq(shear)}$ and $\Delta\theta$ in No. 4 are almost the same magnitude and distribution as those in No. 9. Consequently, even if the L_d/t_d is the same value, the strain imposed by rolling does not exhibit exactly the same magnitude and distribution through sheet thickness because the deformation behaviors during rolling are not simple due to the effect of the shear deformation. Under the L_d/t_d =5.1, the $\varepsilon_{eq(shear)}$ increases with increasing r for the same t_0. However, provided that the L_d/t_d is employed under the same r, the ε_{eq} through sheet thickness agrees regardless of the combination of t_0 and d^ϕ in the friction coefficient range of $\mu \le 0.25$. For high friction of $\mu \ge 0.3$, the ε_{eq} at locations from 1/4 thickness to the surface becomes larger as t_0 decreases, and this tendency becomes more remarkable with increasing μ.

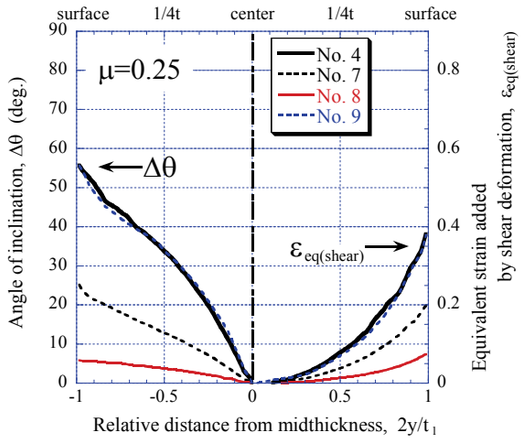

Fig. 15. Distributions of $\Delta\theta$ (lefthand side) and $\varepsilon_{eq(shear)}$ (righthand side) through sheet thickness in rolled Al with μ=0.25 under L_d/t_d =5.1.

As a result, the L_d/t_d parameter shown in Fig. 1 should be expressed by the following equation including t_0, d^ϕ and r, using the relation of $t_1=t_0/(1-r)$.

$$\frac{L_d}{t_d} = \frac{1}{2-r}\sqrt{\frac{2dr}{t_0}} \tag{4}$$

The relation among the roll bite geometry L_d/t_d, roll diameter d^ϕ, nominal reduction r, and initial thickness t_0 is plotted in Fig. 16 for various combinations of d^ϕ, r, and t_0. Here, the open symbols indicate the rolling conditions employed in the literature related to the microstructure change through sheet thickness in a rolling process, including ARB. The L_d/t_d gradually increases with increasing d^ϕ under constant t_0 and r (Fig. 16(a)) and monotonically increases with increasing r under constant d^ϕ and t_0 (Fig. 16(b)). Under d^ϕ and r constant (Fig. 16(c)), the L_d/t_d gradually increases with decreasing t_0, and there is a steep increase at t_0 < 5 mm. Compared to the increases of d^ϕ or r, the decrease of t_0 has a large influence on the increase of L_d/t_d. It is found from Fig. 16 that the L_d/t_d is different with regard to t_0, d^ϕ, and r. Even if the friction condition is the same, this causes the

difference in the magnitude and distribution of strains, as shown in the present study, which results in the changes of the microstructure and texture depending on the thickness location of a rolled sheet.

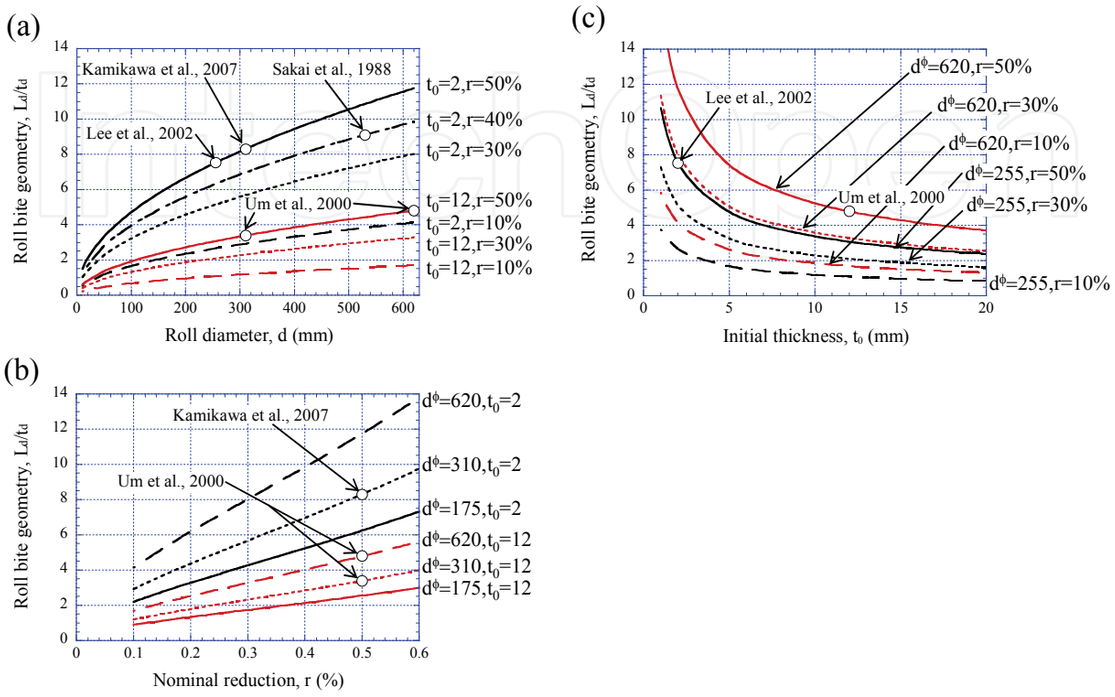

Fig. 16. Variations of the roll bite geometry L_d/t_d with (a) roll diameter d^{ϕ}, (b) nominal reduction r, and (c) initial thickness t_0. Here, the open symbols indicate the rolling conditions employed in the literature.

4. Outlook

It is commonly accepted that the distribution of the equivalent strain through thickness in a rolled sheet depends on the presence of shear deformation due to friction between the rolls and the sheet and brings about a change of microstructure (grain size, texture) through sheet thickness. It is found from the present results that the roll bite geometry defined by equation (4), as well as the friction coefficient, is an important parameter for studying microstructural changes through thickness in metal sheet rolling including ARB process. The grain size decreases with an increase of the equivalent strain, and, hence, a rolling condition with high reduction using a mill with a large roll diameter without a lubricant is effective for the refinement of crystal grains. Such rolling conditions can be seen in hot rolling (high friction and large roller) rather than cold rolling (low friction condition and small roller) and in a commercial rolling mill of product level (large roller) rather than a rolling mill of laboratory level (small roller). Moreover, the microstructural evolution depends strongly on not only equivalent strain but also shear strain. Inoue et al., 2002 reported that in the ferrite grain transformed from deformed austenite, the grain size in the area with the shear strain is finer than that in the area without the shear strain under the same equivalent plastic strain. Cho et al., 2004; Kang et al., 2010 demonstrated significant advances in high angle grain

boundaries and the subdivision of grains under the deformation with shear strain than under without shear strain using Ni-30Fe alloy and low carbon steel. In other words, it is noted that the shear deformation plays a important role for refining crystal grains.
Also, it is known that a shear texture different from a conventional rolling texture develops at the locations where shear deformation is introduced by rolling. Control technology of texture associated with the shear deformation is positively used to improve the deep drawability (ND//<111>) and magnetic characteristic (Goss orientation: {110}<001>). The texture of ND//<111>, which contributes to improve the deep drawability, is produced by a large shear deformation in fcc metals, but its deformation is disadvantageous in bcc metals (Matsuo, 1989). Therefore, for a study of deep drawability, using a large roller is important for the case of aluminum alloys (fcc), and a small roller is recommended for the case of IF steels (bcc). In study of deep drawability in ferritic rolling of extra low carbon steels, Kawabe et al., 1996 reported that the r-value in the sheet improved more significantly when using a small than a large roller under the same friction condition. They confirmed, using the embedded-pin method, that the improvement in the r-value was the result of the decrease of the shear deformation through sheet thickness. Consequently, in order to study universal relation between microstructure (grain size, texture) and plastic deformation, it is essential to understand the quantity (magnitude) and quality (component) of the strain into materials introduced by a plastic deformation process through a combination of numerical simulations and experimental measurements and observations. And a quantitative relation among the strains, friction, and roll bite geometry obtained from numerical simulations would provide useful guidelines for studying the microstructure design in a rolled sheet and for understanding the quantitative correlation between microstructures and strain in ARB process.

5. Conclusions

The effect of the roll bite geometry, L_d/t_d, on the magnitude and distribution of strains imposed in a metal sheet by rolling under various friction conditions was studied using a finite element simulation that takes the deformation history into account. The relation among the strains, distance from center in RD, ΔL, and angle of inclination from the y axis, $\Delta\theta$, was shown through thickness in a rolled 1100 Al. The present results will provide useful guidelines for studying the correlation between microstructures and strain in accumulative roll-bonding (ARB) process as well as the microstructure design in a rolled sheet. The main results are as follows:

1. The deformation through sheet thickness during and after rolling depends strongly on not only the friction condition between the rolls and the sheet but also the roll bite geometry L_d/t_d. The L_d/t_d ratio has a similar effect on friction coefficient μ regarding the relation among ε_{eq}, ΔL, and $\Delta\theta$ through sheet thickness after rolling. In other words, the roll bite geometry is as important a processing parameter as the friction condition for studying microstructural changes through thickness in metal sheet rolling and ARB process.
2. The ε_{eq} in a rolled sheet gradually increases toward the surface from the center and shows a distribution with the maximum at the surface. The maximum ε_{eq} increases with increasing μ or L_d/t_d. On the other hand, in the total shear strain γ, there is a sudden

dip at the thickness location near surface under high friction condition. This behavior is attributed to the decrease in the reverse shear strain γ– induced by the shear stress after a neutral plane.

3. Under different values of the friction coefficient or roll bite geometry, the equivalent strain ε_{eq} had much better correlation with the ΔL and $\Delta\theta$ through sheet thickness, except near the surface, than the total shear strain γ. This is attributed to the fact that ΔL and $\Delta\theta$ are determined by a combination of strains in the x and y directions and the shear strain and their histories during rolling.
4. The L_d/t_d is expressed by equation including initial thickness, t_0, roll diameter, d^{ϕ}, and nominal reduction, r. The L_d/t_d at the same r can be employed as a universal parameter on the equivalent strain in a rolled sheet, except for thickness locations near the surface under high friction conditions.
5. In ARB process, which half of the sheet-surface regions comes to the center in the next cycle and its procedure is repeated, a rolling condition with large roll bite geometry at a high friction condition is desirable for fabricating ultrafine-gained materials efficiently.

6. References

ABAQUS/Explicit ver. 6.5 User's manual, Theory manual; (2006). Providence, ABAQUS Inc., CD-ROM.

Ataka, M., (2006). *Handbook of Technology of Plasticity*, Corona Publishing Co., Ltd., Tokyo, pp. 11-131.

Backofen, W.A., 1972. *Deformation Processing*, Addison-Wesley Pub. Co., Massachusetts, pp. 94-115.

Cho, J.Y., Inoue, T., Yin, F. & Nagai, K. (2004). Effect of shear deformation on microstructural evolution of Ni-30Fe alloy during hot deformaiton. *Materials Transactions,* Vol. 45, pp. 2966-2973.

Cui, Q. & Ohori, K. (2000). Grain refinement of high purity aluminium by asymmetric rolling. *Materials Science and Technology*, Vol. 16, pp. 1095-1101.

Dieter, G.E., 1988. *Mechanical Metallurgy SI Metric Edition*, McGraw-Hill Book Co., 0-07-100406-8, Singapore, pp. 501-563.

Hashimoto, S., Tsukatani, I., Kashima, T. & Miyoshi, T. (1998). Development of hot-rolled steel sheet with a high r-value by rolling in ferrite region with lubrication. *Kobe Steel Engineering Reports*, Vol. 48, pp. 14-18.

Hidalgo, P., Cepeda-Jiménez, C.M., Ruano, O.A. & Carreño, F. (2010). Influence of the Processing Temperature on the Microstructure, Texture, and Hardness of the 7075 Aluminum Alloy Fabricated by Accumulative Roll Bonding. *Metallurgical and Materials Transactions A*, Vol. 41, pp. 758-767.

Horita, Z., Fujinami, T., Nemoto, M. & Langdon, T.G. (2000). Equal-channel angular pressing of commercial aluminum alloys: grain refinement, thermal stability and tensile properties. *Metallurgical and Materials Transactions A*, Vol. 31, pp. 691-701.

Inoue, T., Torizuka, S., Nagai, K., Tsuzaki, K. & Ohashi, T. (2001). Effect of plastic strain on grain size of ferrite transformed from deformed austenite in Si-Mn steel. *Materials Science and Technology*, Vol. 17, pp. 1580-1588.

Inoue, T., Torizuka, S. & Nagai, K. (2002). Effect of shear deformation on refinement of crystal grains. *Materials Science and Technology*, Vol. 18, pp. 1007-1015.

Inoue, T., Ochiai, T., Yin, F. & Nagai, K. (2007a). Test production of ultrafine-grained steel plate by large-scale forging press. *Tetsu-to-Hagane*, Vol. 93, pp. 693-702.

Inoue, T., Yin, F. & Kimura, Y. (2007b). Strain distribution and microstructural evolution in multi-pass warm caliber rolling. *Materials Science and Engineering A*, Vol. 466, pp.114-122.

Inoue, T., Horita, Z., Somekawa, H. & Ogawa, K. (2008). Effect of initial grain sizes on hardness variation and strain distribution of pure aluminum severely deformed by compression tests *Acta Materialia*, Vol. 56, pp. 6291-6303.

Inoue, T., Todaka, Y. & Horita, Z. (2009a). Special issue on severe plastic deformation for production of ultrafine structures and unusual mechanics properties: understanding mechanisms. *Materials Transactions*, Vol. 50, pp. 1-116.

Inoue, T. & Tsuji, N. (2009b). Quantification of strain in accumulative roll-bonding under unlubricated condition by finite element analysis. *Computational Materials Science*, Vol. 46, pp. 261-266.

Inoue, T., Somekawa, H. & Mukai, T. (2009c). Hardness variation and strain distribution in magnesium alloy AZ31 processed by multi-pass caliber rolling. *Advanced Engineering Materials*, Vol. 11-8, pp. 654-658.

Inoue, T., Yin, F., Kimura, Y., Tsuzaki, K. & Ochiai, S. (2010a). Delamination effect on impact properties of ultrafine-grained low carbon steel processed by warm calibre rolling. *Metallurgical and Materials Transactions A*, Vol. 41-2, pp. 341-355.

Inoue, T., Yin, F. & Kimura, Y. (2010b). Effect of deformation mode on texture of ultrafine-grained low carbon steel processed by warm caliber rolling. *Materials Science Forum*, Vols. 638-642, pp 2793-2798.

Kamikawa, N., Sakai, T. & Tsuji, N. (2007). Effect of redundant shear strain on microstructure and texture evolution during accumulative roll-bonding in ultralow carbon IF steel. *Acta Materialia*, Vol. 55, pp. 5873-5888.

Kang, J-.H., Inoue, T. & Torizuka, S. (2010). Effect of shear strain on the microstructural evolution of a low carbon steel during warm deformation. *Materials Transactions*, Vol. 51, pp. 27-35.

Kawabe, H., Matsuoka, S., Seto, K., Sakata, T., Furugimi, O. & Ohara, T. (1996). Effect of roll diameter on deep drawability of extra low C sheet steels with hot rolling at ferrite region. *CAMP-ISIJ*, Vol. 9, p. 1333.

Kimura, Y., Inoue, T., Yin, F. & Tsuzaki, K. (2008). Inverse temperature dependence of toughness in an ultrafine grain structure steel. *Science*, Vol. 320, pp. 1057-1060.

Kolahi, A., Akbarzaden, A. & Barnett, M.R. (2009). Electron back scattered diffraction (EBSD) characterization of warm rolled and accumulative roll bonding (ARB). *J. Materials Processing Technology*, Vol. 209, pp. 1436-1444.

Lee, S.H., Saito, Y., Tsuji, N., Utsunomiya, H. & Sakai, T. (2002). Role of shear strain in ultragrain refinement by accumulative roll-bonding (ARB) process. *Scripta Materialia,* Vol. 46, pp. 281-285.

Matsuo, M. (1989). Texture control in the production of grain oriented silicon steels. *ISIJ International*, Vol. 29, pp. 809-827.

Matsuoka, S., Morita, M., Furukumi, O. & Obara, T. (1997). Structural variation along thickness direction of extra-low carbon sheet steels rolled in ferrite region. *Tetsu-to-Hagane*, Vol. 83, pp. 127-132.

Mukai, T., Somekawa, H., Inoue, T. & Singh, A. (2010). Strengthening Mg–Al–Zn alloy by repetitive oblique shear strain with caliber roll. *Scripta Materialia,* Vol. 62, pp. 113-115.

Mukhopadhyay, A, Higginson, R.L., Howard, I.C. & Sellars, C.M. (2007). Strain summation in finite element modeling of multipass hot rolling. *Materials Science and Technology*. Vol.23-1 pp.29-37.

Saito, Y., Tsuji, N., Utsunomiya, H., Sakai, T. & Hong, R.G. (1998). Ultra-fine grained bulk aluminum produced by accumulative roll-bonding (ARB) process. *Acta Materialia*, Vol. 39, pp. 1221-1227.

Sakai, T., Saito, Y., Hirano, K. & Kato, K. (1988). Recrystallization and texture formation in high speed hot rolling of austenitic stainless steel. *Trans ISIJ,* Vol. 28, pp. 1028-1035.

Sakai, T. & Saito, Y. (1999). Effect of inhomogeneous deformation throgh the thickness on microstructure and texture of hot rolled sheet. *J. Japan Society Technology Plasticity*, Vol. 40, pp. 1158-1163.

Segal, V.M. (1995). Materials processing by simple shear. *Materials Science and Engineering A*, Vol. 197, pp.157-164.

Todaka, Y., Inoue, T. & Horita, Z. (2008). Special issue on severe plastic deformation for production of ultrafine structures and unusual mechanics properties: Investigating role of high-density lattice defects. *Materials Transactions,* Vol. 49, pp. 1-106.

Um, K.-K., Jeong, H.-T., An, J.-K., Lee, D.N., Kim, G. & Kwon, O. (2000). Effect of initial sheet thickness on shear deformation in ferritic rolling of IF-steel sheets. *ISIJ International*, Vol. 40, pp. 58-64.

Underwood, L.R. (1952). *The Rolling of Metals*. Chapman&Hall Ltd., London, pp. 57-93, 203-268.

Utsunomiya, H., Tanda, K., Saito, Y., Sakai, T. & Tsuji, N. (1999). *J. Japan Society Technology Plasticity*, Vol. 40, pp. 1187-1191.

Xing, Z.P., Kang, S. B. & Kim, H.W. (2002). Microstructural evolution and mechanical properties of the AA8011 alloy during the accumulative roll-bonding process. *Metallurgical and Materials Transactions A*, Vol. 33, pp. 1521-1530.

Zhang, X.J., Hodgson, P.D. & Thomson, P.F. (1996). The effect of through-thickness strain distribution on the static recrystallization of hot rolled austenitic stainless steel strip. *Materials Processing Technology*, Vol. 60, pp. 615-619.

Finite Element Analysis

Edited by David Moratal

ISBN 978-953-307-123-7

Hard cover, 688 pages

Publisher Sciyo

Published online 17, August, 2010

Published in print edition August, 2010

Finite element analysis is an engineering method for the numerical analysis of complex structures. This book provides a bird's eye view on this very broad matter through 27 original and innovative research studies exhibiting various investigation directions. Through its chapters the reader will have access to works related to Biomedical Engineering, Materials Engineering, Process Analysis and Civil Engineering. The text is addressed not only to researchers, but also to professional engineers, engineering lecturers and students seeking to gain a better understanding of where Finite Element Analysis stands today.

InTech Europe

University Campus STeP Ri
Slavka Krautzeka 83/A
51000 Rijeka, Croatia
Phone: +385 (51) 770 447
Fax: +385 (51) 686 166
www.intechopen.com

InTech China

Unit 405, Office Block, Hotel Equatorial Shanghai
No.65, Yan An Road (West), Shanghai, 200040, China
中国上海市延安西路65号上海国际贵都大饭店办公楼405单元
Phone: +86-21-62489820
Fax: +86-21-62489821

IntechOpen